J. Fluid Mech. (1970), *vol.* 42, *part* 1, *pp.* 1–15
Printed in Great Britain

The turbulent boundary layer on a rotating cylinder in an axial stream

By T-S. CHAM† AND M. R. HEAD‡
Cambridge University Engineering Department

(Received 11 December 1968 and in revised form 9 December 1969)

Calculations are presented of the development of the turbulent boundary layer on a rotating cylinder with its axis along the stream, and the results are compared with measurements made by Parr. With the choice of a suitable co-ordinate system, the boundary layer downstream of the nose of the cylinder approximates closely to a condition of two-dimensionality, and a simple integral method of solution can be applied. The only evidence of three-dimensionality lies in the destabilizing effect of rotation on the turbulence structure of the layer and an analysis of this instability has been made which relates changes in mixing length and entrainment to an instability parameter in the form of a Richardson number.

In spite of the changes in shear stress distribution and entrainment brought about by rotation, mean velocity profiles and skin friction values are found to be related to H and R_θ in the same way as for the stationary flat plate.

1. Introduction

Examples of boundary-layer flow on a body of revolution rotating in an axial stream are to be found in several engineering applications; for example, in the flow over an airscrew spinner, or a rotating projectile, or the rotating hubs of various types of turbo-machine. In most circumstances the boundary layer will be turbulent, either because of high stream turbulence or because of the destabilizing effects of rotation on the laminar boundary layer. The prediction of turbulent boundary-layer development is therefore required if an accurate assessment is to be made of torque and drag.

One of the most evident characteristics of the boundary layer on a body rotating in a stream is the skewness of the velocity profile, as shown in figure 1. Because of the boundary conditions, the velocity vector must turn through a right angle in tracing the velocity through the layer. At first sight, this three-dimensionality would appear to complicate the problem, and indeed this is generally true. However, it can be shown theoretically that, for the special case of the rotating circular cylinder investigated here, the boundary-layer flow can be reduced effectively to two dimensions by a suitable choice of axes rotating with the cylinder. This result was pointed out by Sutton (Horlock, Norbury &

† Present address: Faculty of Engineering, University of Singapore.
‡ Present address: Indian Institute of Technology, Kanpur.

Cooke 1967) and has been demonstrated by the measurements of Parr (1962) and Furuya, Nakamura & Kawachi (1966). In fact, Parr, who first observed this behaviour experimentally, simply commented on the result as 'remarkable' and used it as an assumption in his subsequent theoretical analysis. Furuya, on the other hand, apparently recognized that the quasi-collateral condition should exist and established the effective two-dimensionality of the flow to within the experimental accuracy of his measurements. However, no attempt was made to explain the occurrence of the two-dimensionality.

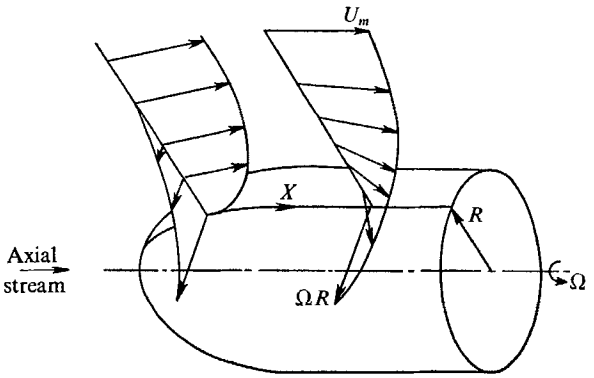

FIGURE 1. Boundary-layer flow on a rotating cylinder in an axial stream.

Physically, the boundary-layer development on a rotating cylinder in an axial stream is equivalent to that on a flat plate with the fluid subjected to outward normal forces. Since the forces are in fact the centrifugal forces, they are dependent on the rate of rotation and an important dimensionless parameter in the problem is the ratio λ, where

$$\lambda = \frac{\text{Circumferential velocity}}{\text{Axial velocity of free stream}} = \frac{\Omega R}{U_m}.$$

In the calculation of the boundary layer for this case, it cannot be assumed with any certainty that the usual properties of a turbulent boundary layer hold good. For example, it is easy to see that centrifugal instability may cause a higher magnitude of velocity fluctuations in the boundary layer and consequently a greater turbulence intensity. As the rate at which irrotational fluid is incorporated into the boundary layer depends, at least in part, on this intensity, it is expected that there should be a higher rate of entrainment. The non-dimensional entrainment has therefore been left as a 'free' parameter in the following calculations although results are also presented based on the unmodified flat-plate entrainment.

In fact, the modification to the entrainment was the only concession made to rotational effects, and the turbulent boundary-layer development was calculated by the straightforward application of the two-dimensional momentum-integral and entrainment equations, using the skin-friction relation and profile family due to Thompson (1965). The results have been compared with the measurements of Parr and, as will be seen later, show very satisfactory agreement.

2. Theory

2.1. *The quasi-collateral condition*

If, for the cylinder rotating in an axial stream, we take a co-ordinate system fixed in the surface of the cylinder, the streamline at the edge of the boundary layer becomes a helix of pitch angle $\cot^{-1}1/\lambda$. In this co-ordinate system, the velocity of the fluid must decrease within the boundary layer and vanish at the surface of the cylinder. Referring to the direction of the streamline at the edge of the boundary layer as the streamwise direction, there is no tendency for cross-flow to develop since the only pressure gradient that exists is normal to the surface and the Coriolis force acts towards the axis of the cylinder. (This involves the usual boundary-layer assumption that the mean flow normal to the surface is small.)

It can therefore be concluded on physical grounds that cross-flow should be absent and that the boundary-layer streamlines should lie in the direction of the external helix.

Cross-flow will, however, be introduced at the nose portion of the cylinder before the parallel section is reached, but this will be suppressed after a sufficient distance by the shear stresses in the boundary layer. This situation is well illustrated by the experimental results of Furuya *et al.* (1966) where the deviation from the quasi-collateral condition is significantly greater in the laminar region than in the turbulent region further downstream. Not only has the cross-flow had less opportunity to decay in the laminar boundary layer which immediately follows the nose portion, but the shear forces producing the decay are very much smaller in laminar than in turbulent flow.

2.2. *Equations*

Consider a set of axes fixed on the surface of the cylinder. The directions of the axes are along the helix formed by the projection of the streamline at the edge of the boundary layer on the cylinder surface, the perpendicular to this helix but still on the surface, and the radial extension normal to the surface. As the cylinder is a developable surface and the helix projections and their orthogonal family are straight lines on this developed surface, the acceleration terms are simply the corresponding terms in the Cartesian co-ordinate system (see Howarth 1951).

Taking s as measured along the helix, n measured on the cylinder perpendicular to the helix, and z measured normal to the surface, and assuming the thickness of the boundary layer is small compared to the radius of the cylinder, it can be deduced that the following equations of mean motion hold for the turbulent boundary layer:

$$u\frac{\partial u}{\partial s}+v\frac{\partial u}{\partial n}+w\frac{\partial u}{\partial z}=-\frac{1}{\rho}\frac{\partial p}{\partial s}+\frac{\partial}{\partial z}\left(\nu\frac{\partial u}{\partial z}-\overline{u'w'}\right), \tag{1}$$

$$u\frac{\partial v}{\partial s}+v\frac{\partial v}{\partial n}+w\frac{\partial v}{\partial z}=-\frac{1}{\rho}\frac{\partial p}{\partial n}+\frac{\partial}{\partial z}\left(\nu\frac{\partial v}{\partial z}-\overline{v'w'}\right) \tag{2}$$

and

$$\partial p/\partial z = O(1). \tag{3}$$

The equation of continuity is

$$\frac{\partial u}{\partial s} + \frac{\partial v}{\partial n} + \frac{\partial w}{\partial z} = 0. \tag{4}$$

The Coriolis terms are neglected since they are very much smaller than the remaining terms.

From equation (3), it is seen that the pressure difference across the boundary layer is only of order δ and can therefore reasonably be ignored. As there is no pressure gradient in the external flow, the terms $\partial p/\partial s$ and $\partial p/\partial n$ can be discarded, and if we now apply the considerations of the previous section to show that the cross flow is everywhere zero, then (1) and (2) become identical to the boundary-layer equations for flow over a flat plate in zero pressure gradient. Hence, in this co-ordinate system, the boundary-layer flow of the present case is effectively two-dimensional. Just as for the flat plate, (2) is actually redundant. Although it is not possible to prove the uniqueness of the solution for vanishing v everywhere, it is certainly a plausible solution, though the possibility of three-dimensional solutions, periodic in the cross-flow direction, cannot be dismissed on either physical or mathematical grounds. It may be noted a similar analysis applies to the laminar case, the effective two-dimensionality of which was pointed out by Sutton (Horlock *et al.* 1967).

The momentum integral equation thus takes the simple form

$$\frac{d\theta_{11}}{ds} = \frac{\tau_w}{\rho U^2}. \tag{5}$$

where θ_{11} is the momentum thickness, τ_w the wall shear stress in the streamwise direction and U the resultant velocity in the free stream (i.e. the vector sum of U_m and ΩR).

2.3. *Auxiliary equation of entrainment*

Head (1958) has suggested that the rate of entrainment of free-stream fluid by the turbulent boundary layer should be simply a function of the velocity defect in the outer part of the layer, which may be measured by the magnitude of the free-stream velocity and some such form parameter as

$$H\,(\equiv \delta^*/\theta) \quad \text{or} \quad H_{\delta-\delta^*}\,(\equiv \delta - \delta^*/\theta),$$

where δ is the boundary-layer thickness, δ^* the displacement thickness and θ the momentum thickness. Thus, for the flat-plate case, it is assumed that the non-dimensional rate of entrainment C_E is given by $d(\delta-\delta^*)/dx = C_E(H_{\delta-\delta^*})$. Here we make the more general assumption that

$$\frac{d}{ds}(\delta-\delta^*) = C_E(\lambda, H_{\delta-\delta^*}), \tag{6}$$

and curves of C_E for different values of λ have been chosen to give satisfactory agreement between calculated and measured boundary-layer developments. These are shown in figure 2.

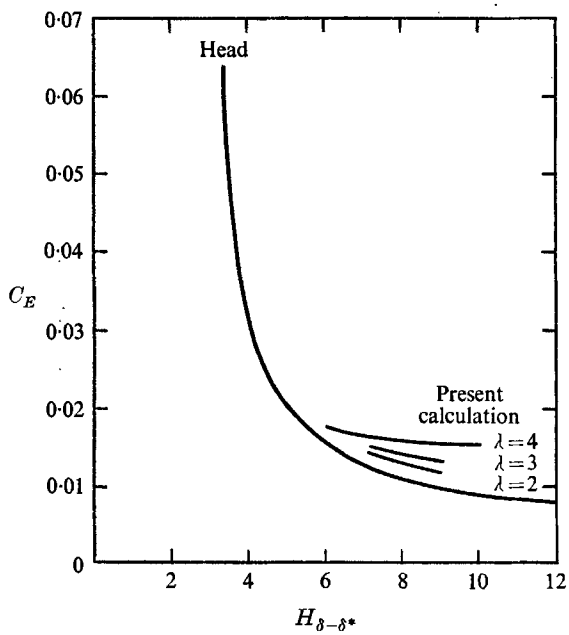

FIGURE 2. Entrainment functions used in present calculations.

3. Method of calculation

To enable solutions to be obtained for (5) and (6) the following assumptions are made: (i) that the mean velocity profiles are essentially similar to those of a normal two-dimensional turbulent boundary layer, i.e. that the profiles can be specified by H and R_θ (where R_θ is the Reynolds number based on momentum thickness) by the use of Thompson's (1965) two-parameter family of velocity profiles. This implies that the centrifugal and Coriolis forces have no direct effect on the mean velocity profiles; (ii) that the skin-friction coefficient is specified by H and R_θ as in the normal two-dimensional boundary layer; i.e. that it is given by Thompson's (1965) skin-friction relationship; (iii) that, although the dependence of $H_{\delta-\delta^*}$ on R_θ is implied by the assumption of a velocity profile family based on H and R_θ, it is sufficiently accurate, for the calculation of H development, to take $H_{\delta-\delta^*}$ as a unique function of H as proposed by Head (1958). This considerably reduces the computational complexity.

The method of solution is one of step-by-step forward calculation from given initial conditions which are obtained from Parr's experiment.

Calculations were carried out for $\lambda = 2, 3$ and 4, the initial point for each calculation being taken within the region where the boundary layer was fully turbulent.

4. Experimental arrangement (Parr 1962)

The results of the calculations were compared with measurements made by Parr and it is therefore appropriate to give a brief description of his experimental arrangement. The rotating body consisted of a rounded nose followed by a

cylindrical section with a constant diameter of 0·456 m, as shown in figure 3. It was rotated in a tunnel of circular section, 0·702 m in diameter, in an axial stream provided by a fan downstream. As it was reported that the measured pressure distribution did not depend upon the rotation parameter, it may be assumed the boundary layers did not have any appreciable blockage effect on the main stream although the clearance between the rotating cylinder and the tunnel wall is not particularly large.

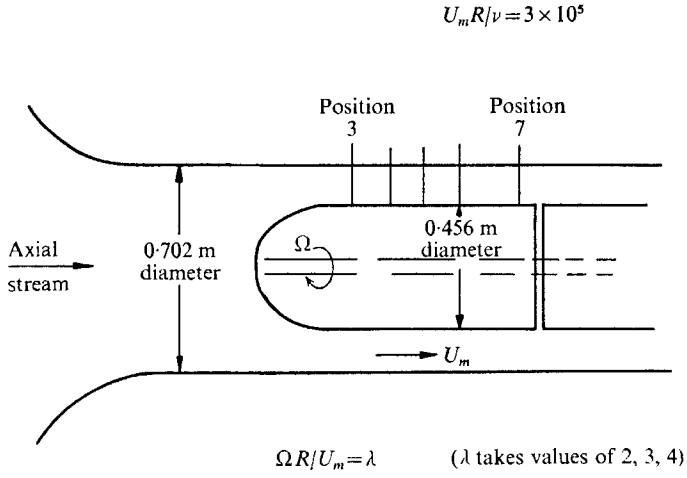

FIGURE 3. Experimental arrangement used by Parr (1962).

Velocity profiles were measured by a 3-hole Pitot tube, and positions of transition from laminar to turbulent flow were determined by means of a hot-wire anemometer. For the sets of experiments used in the present comparisons, the stream velocity in the test section was 20 m s^{-1}, which corresponds to a Reynolds number U_mR/ν of 3×10^5. Although the range of the experiments covered values of the rotation parameter λ from 1 to 4, the set for $\lambda = 1$ has been omitted because of the very small extent of turbulent boundary layer on the body.

An interesting feature of the experiment was that, at a value of λ between 3 to 4, the mean fluctuation velocities were found to be as high as 20 % of the free-stream velocity. This was of course a result of the destabilizing effect of the centrifugal forces mentioned earlier.

5. Comparison between theory and experiment

As the calculations were restricted to the special case of the turbulent boundary layer on a cylinder of constant radius in zero pressure gradient, measurements at stations 0 to 2 were excluded, as they did not lie within the constant pressure region. However, from the experimental pressure distributions given by Parr, it appeared that, from station 3, the pressure remained substantially constant for all λ.

Figure 4 shows, for different values of λ, the calculated curves for the momentum thickness Reynolds number in the streamwise direction, $U\theta_{11}/\nu$, together

with the experimental values. The initial values for the calculations have been taken from the experiments. It is seen that the agreement between the calculations and the experiments is satisfactory even without any change in the entrainment relation given by Head. However, as will be seen from figure 5, where calculated and experimental values of the form parameter of the streamwise velocity profiles are compared, the agreement is greatly improved when the entrainment

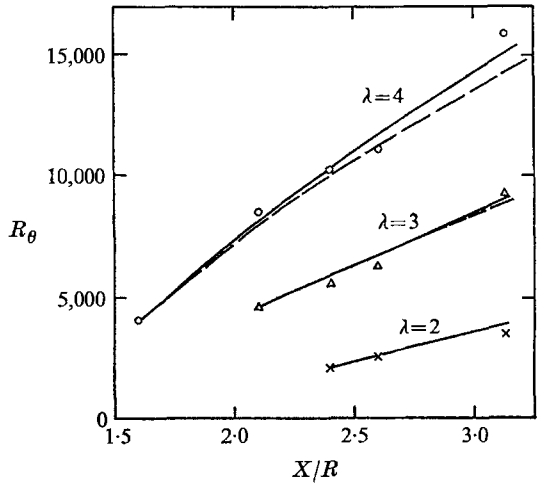

FIGURE 4. Developments of momentum thickness Reynolds number. ———, present calculation; — —, from Head's (1958) entrainment; ○, △, ×, experiment.

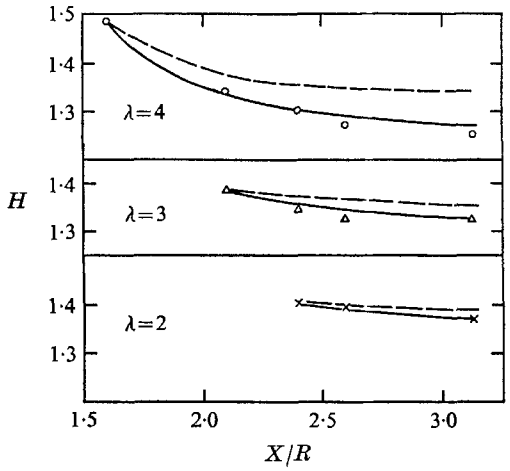

FIGURE 5. Developments of the boundary-layer form parameter. ———, present calculation; — —, from Head's (1958) entrainment; ○, △, ×, experiment.

rate is appropriately increased. This is because the form-parameter development is more sensitive to changes in entrainment than is the momentum-thickness development.

The velocity profiles, as given by Thompson's two-parameter family for calculated H, R_θ values, agree closely with those measured by Parr, as shown in figure

6 for position 5 and different values of λ. This indicates, that, although the boundary layer may have an appreciably higher turbulence level, the mean velocity profile is still quite similar to that of a normal two-dimensional turbulent boundary layer having the same values of H and R_θ.

The torque coefficient C_M is given by

$$C_M = \frac{M}{\frac{1}{2}\rho\Omega^2 R^5},$$

where M is the total resisting moment from the stagnation point to the point under consideration.

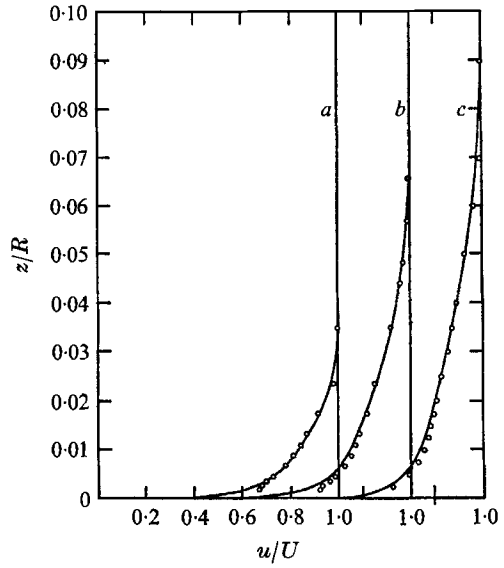

FIGURE 6. Velocity profiles for position 5 (X/R = 2·4) at different rates of rotation. O, experiment; ———, theory.

	a	*b*	*c*
H	1·40	1·36	1·30
$R_{\theta_{11}}$	2075	5900	10250
λ	2	3	4

This quantity was deduced by Parr from the measurements of mean velocity profiles by equating the rotational momentum loss to the applied moment. As shown in figure 7, the agreement between the present calculations and the experimental deductions is satisfactory, indicating that the $c_f(H, R_\theta)$ relation given by Thompson is adequate for application to this rotating flow. The high boundary-layer turbulence and the curved surface do not appear to have any noticeable effect on the wall friction value.

The overall agreement shows that all the assumptions made are justifiable, and that such an integral method of solution should be sufficiently accurate for engineering purposes.

6. Analysis of the instability in the boundary layer

6.1. *Introduction*

There is considerable current interest in the effects of surface curvature on boundary-layer development. As the detailed experimental data for the rotating cylinder is available, along with a satisfactory analytical description of the flow, it should be possible to obtain information regarding the effects of destabilizing centrifugal forces on the turbulent boundary layer.

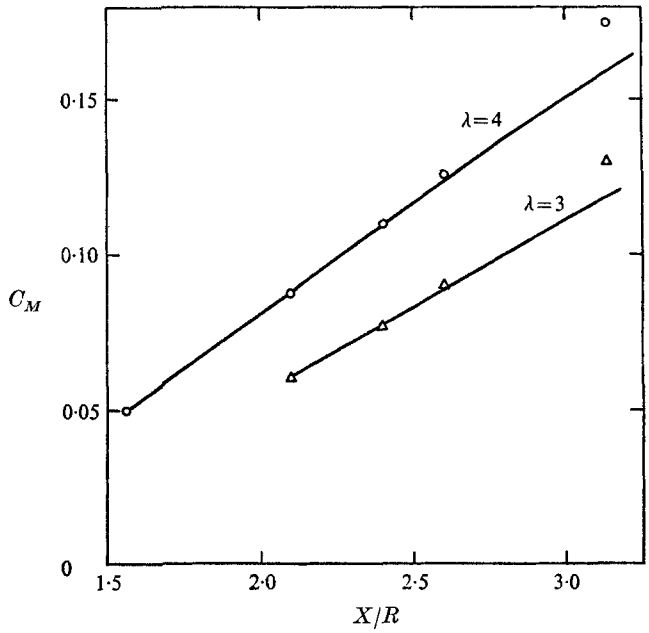

FIGURE 7. Torque coefficients of the rotating cylinder. $C_M = M/\frac{1}{2}\rho\Omega^2R^5$. ———, theory; ○, △, experiment.

Bradshaw (1969) showed that, physically, an appropriate Richardson number can be considered as the ratio of the square of the Brunt–Väisälä frequency to the square of the turbulence frequency. To derive the Brunt–Väisälä frequency, the flow is considered relative to a set of axes fixed in space. Referring to figure 8, it is easily seen that the stability of the axial component should not be substantially affected by the rotation, as it is qualitatively not much different from the flow over a flat plate. On the other hand, the circumferential component is subjected to centrifugal forces and is delicately balanced by normal pressure gradient. This highly unstable situation gives rise to large fluctuations.

If the turbulence frequency is to be represented by some eddy-frequency scale, the appropriate scale in this particular case is obviously the gradient of the resultant velocity with respect to an axis rotating with the cylinder.

The analogous Richardson number is therefore

$$Ri = \frac{2v^*}{r^2}\frac{\partial(v^*r)}{\partial r}\Big/\left(\frac{\partial u}{\partial r}\right)^2. \tag{7}$$

Bradshaw (private communication) gave an equivalent expression of the Richardson number for this particular flow:

$$Ri = \left[\frac{2\lambda^2}{1+\lambda^2}\right]\left[\frac{U_m}{R}\left(1-\frac{u_1}{U_m}\right)\Big/\frac{\partial u_1}{\partial r}\right].$$

This is a simplified form of (7) incorporating the additional assumption that curvature effects are small (i.e. $\partial u_1/\partial r \gg u_1/R$).

A typical distribution of the Richardson number in the turbulent boundary layer of the rotating cylinder is given in figure 9.

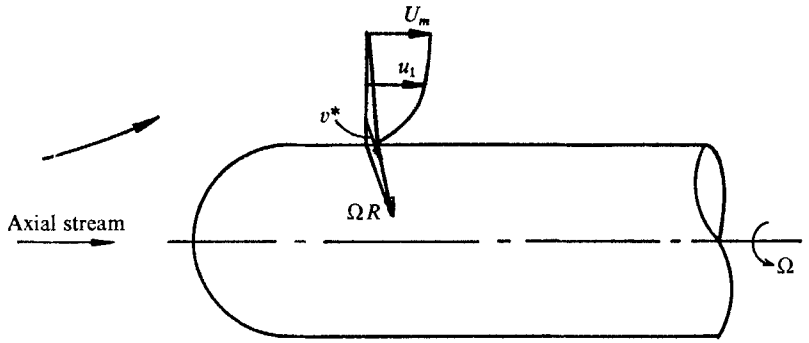

FIGURE 8. Velocity components of the boundary-layer flow with respect to a fixed co-ordinate system.

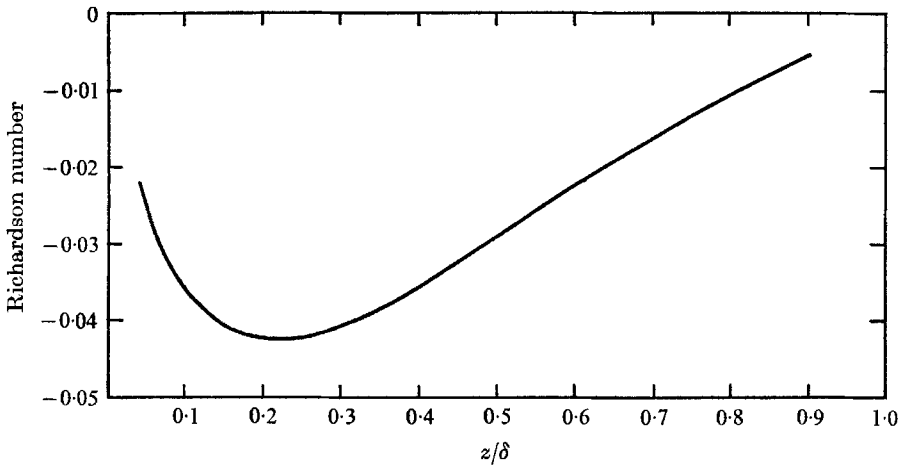

FIGURE 9. A typical distribution of the Richardson number in the turbulent boundary layer on a rotating cylinder.

6.2. *Estimation of changes in the apparent mixing length*

In the Earth's boundary layer, the change in the apparent mixing length has been expressed by the Monin–Oboukhov formula

$$\frac{l}{l_0} = 1-\beta Ri,$$

where β is a constant, roughly equal to 7 in stable conditions and 4·5 in unstable conditions.

However, there is no *a priori* evidence that the same constant β should apply, or that β should not vary across the boundary layer. For this reason it is of interest to determine values of β by evaluating the other terms in the above formula.

The Richardson number can readily be obtained from expression (7) if the velocity profile is known. Evaluation of the ratio of mixing lengths, on the other hand, needs special consideration, since it requires a knowledge of the shear stress distribution in the boundary layer both for the case with instability and for the case without. Moreover, similar local conditions are required in the two cases (i.e. similar values of H and R_θ), so that the change in mixing length is entirely due to instability.

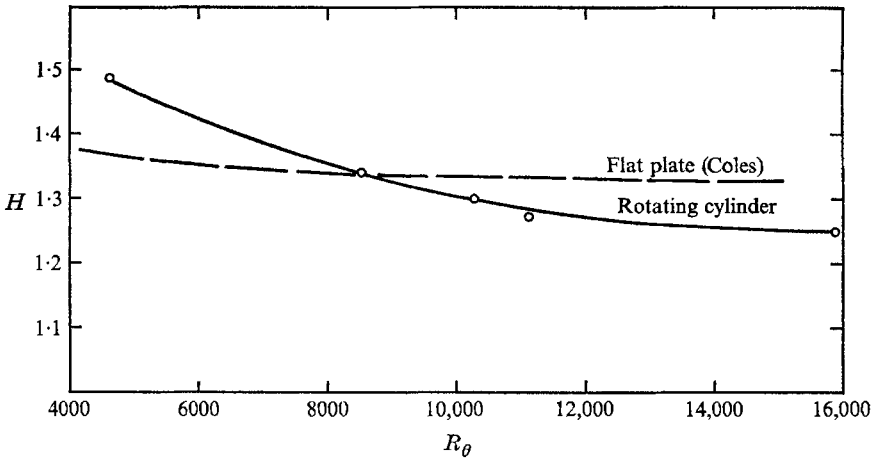

FIGURE 10. Development of the turbulent boundary layer on a flat plate and on a rotating cylinder ($\lambda = 4$). O, experiment; ———, present calculation.

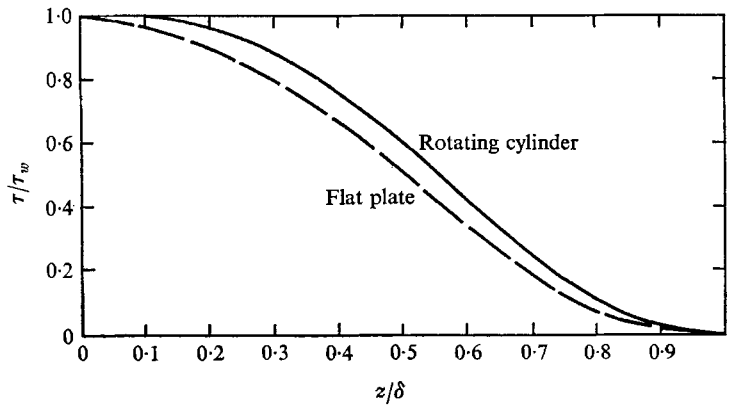

FIGURE 11. Calculated shear-stress profiles for the turbulent boundary layer on a flat plate and on a rotating cylinder ($\lambda = 4$). $H = 1{\cdot}34$, $R_\theta = 8500$.

Referring to figure 10, the plot of H against R_θ shows that there is an identical point for comparison in the developments of the turbulent boundary layers for the rotating cylinder ($\lambda = 4$) and the flat plate. This corresponds to an H of 1·34 and R_θ of 8500.

As the boundary-layer developments are given, the shear stress profiles can be evaluated assuming the velocity profiles to be represented by Thompson's family. The shear stress distributions determined in this way are shown in figure 11.

As mixing-length theory gives

$$\tau = \rho l^2 (\partial u/\partial z)^2,$$

it is easily deduced that for similar velocity profiles and boundary-layer thicknesses

$$l/l_0 = \sqrt{(\tau/\tau_0)},$$

where the suffix 0 refers to the flat plate conditions. The constant β is therefore evaluated from

$$\beta = \frac{1-\sqrt{(\tau/\tau_0)}}{Ri}.$$

Profiles of l/l_0 and β are given in figure 12. It is seen that β varies from about 0·25 near the wall to approximately 60 near the outer edge. It may be noted that the calculation becomes more unreliable as the edge of the boundary layer is

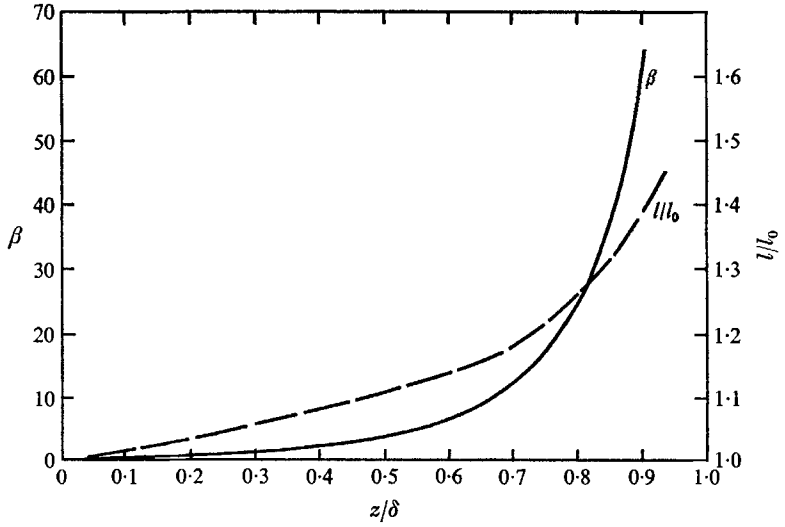

FIGURE 12. Calculated l/l_0 and β profiles in the turbulent layer.

approached, due to the difficulty of evaluating the shear stress with the necessary accuracy in this region. An important result is that the usual constant of $\beta = 4{\cdot}5$ for unstable conditions, as used in meteorology, seems to apply only at the mid-region of the turbulent boundary layer.

6.3. *Correlation between instability in the turbulent boundary layer and increase in entrainment*

It may reasonably be assumed that the rate of entrainment depends upon the velocity defect of the outer part of the boundary layer and the turbulence level within the boundary layer. As the velocity defect can be represented by $\partial u/\partial z$

and the turbulence level by the mixing length l, the rate of entrainment might be expected, by dimensional arguments, to be proportional to $l(\partial u/\partial z)$ (cf. Sawyer 1963).

Since the entrainment occurs in the intermittent region, it is logical to determine effects on the rate of entrainment by referring to conditions at the centre of this region. (See Sawyer 1963.) From the measurements of intermittency by Fiedler & Head (1966), it is seen that the centre of this region varies between $y/\delta = 0{\cdot}8$ and $y/\delta = 0{\cdot}9$. The value of 0·8 seems to apply for most turbulent boundary layers but for one near separation or with an exceptionally high level of turbulence it is nearer to 0·9.

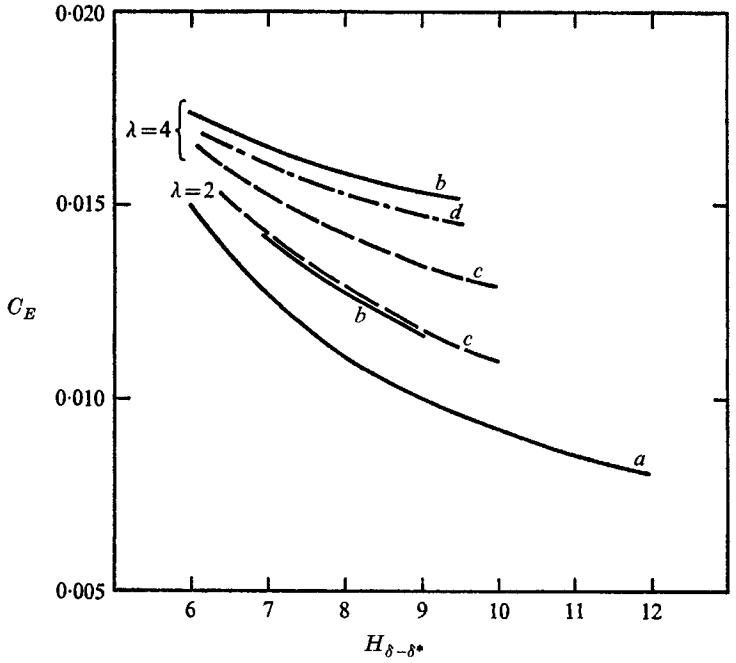

FIGURE 13. Entrainments as a function of $H_{\delta-\delta^*}$. Curves: *a*, Head; *b*, curves used in calculations; *c*, $C_E = C_{E0}\,(1-25Ri_{y/\delta=0.8})$; *d*, $C_E = C_{E0}\,(1-60\,Ri_{y/\delta=0.9})$.

For the present, it is assumed that the rate of entrainment is represented by the conditions at $y/\delta = 0{\cdot}8$, both for the unstable turbulent boundary layer and the neutrally stable flat-plate turbulent boundary layer.

Based on this assumption, the ratio of the entrainments for the same H and R_θ is easily deduced to be

$$C_E/C_{E0} = (1-\beta\,{}^*Ri), \tag{8}$$

where C_E is the entrainment for the unstable case,

C_{E0} is the entrainment for the stable case,

$^*Ri$ is the Richardson number at $y/\delta = 0{\cdot}8$.

and $\beta = 25$ (see figure 12).

Using the above formula, the 'theoretical' entrainment curves are plotted for $\lambda = 2$ and 4 in figure 13. It is seen that the agreement between the above formula and the curves actually used is good for $\lambda = 2$, but about 15% low for $\lambda = 4$. A possible explanation is that, at this higher rate of rotation, the centre of the entraining layer is nearer to $y/\delta = 0{\cdot}9$ than 0·8. A formula based on this conjecture gives considerably improved agreement, as shown in figure 13.

It is admitted that the method of correlation is highly empirical and there is need for more experiment. However, it does seem to give a fair estimate of the order of magnitude of the increase in entrainment. Until it is superseded by more accurate analysis, (8) should be useful for application to other types of unstable boundary-layer flow, such as that over a concave surface.

7. Conclusions

It has been shown that, by the transformation to a set of axes rotating with the cylinder, the equations reduce to those for a two-dimensional boundary layer, provided the thickness of the layer is small compared to the radius of the cylinder.

By merely increasing the rate of entrainment to take account of centrifugal instability, the normal two-dimensional turbulent boundary-layer calculation method proposed by Head can be used to obtain accurate predictions of the development of form parameter and momentum thickness. In addition, Thompson's two-dimensional velocity profile family gives a good description of the velocity profiles measured relative to a set of rotating axes.

The instability in the turbulent boundary layer on a rotating cylinder can be expressed as a Richardson number in the same way as for thermal instability. Correlation between the ratio of mixing lengths and the Richardson number seems to indicate not a constant β of 4·5 in the Monin–Oboukhov formula, but a range of values from 0·25 to approximately 60 across the turbulent boundary layer. The increase in entrainment can be approximately described by the formula $C_E = C_{E0}(1 - \beta^* Ri)$, where β has the value of about 25 corresponding to the Richardson number $^*Ri$ being evaluated at $y/\delta = 0{\cdot}8$.

REFERENCES

Bradshaw, P. 1969 The analogy between streamline curvature and buoyancy in turbulent shear flow. *J. Fluid Mech.* **36**, 177.

Fiedler, H. E. & Head, M. R. 1966 Intermittency measurements in the turbulent boundary layer. *J. Fluid Mech.* **25**, 719.

Furuya, Y., Nakamura, I. & Kawachi, H. 1966 The experiment on the skewed boundary layer on a rotating body. *Japan Soc. Mech. Engng Bull.* **9**, 36, 702.

Head, M. R. 1958 Entrainment in the turbulent boundary layer. *Aero. Res. Counc. R & M* 3152.

Horlock, J. H., Norbury, J. F. & Cooke, J. C. 1967 Three-dimensional boundary layers: a report on Euromech 2. *J. Fluid Mech.* **27**, 369.

Howarth, L. 1951 The boundary layer in three-dimensional flow. Part I. Derivation of the equations for flow along a general curved surface. *Phil. Mag.* (7), **42**, 239.

PARR, O. 1962 Untersuchungen der dreidimensionalen Grenzschicht an rotierenden Drehkörpern bei axialer Anströmung. Ph.D. Thesis, Institute of Fluid Mechanics, Braunschweig Technical University. See also 1963 *Ing. Arch.* **32**, 393.

SAWYER, R. A. 1963 Two-dimensional reattaching jet flows including the effects of curvature on entrainment. *J. Fluid Mech.* **17**, 481.

THOMPSON, B. G. J. 1965 A new two-parameter family of mean velocity profiles for incompressible turbulent boundary layers on smooth walls. *Aero. Res. Counc. R & M* 3463.